

Structured randomness: Jamming of soft discs and pins

Prairie Wentworth-Nice,^{a‡} Sean Ridout,^b Brian Jenike,^a and Amy L. Graves^{*a}

Simulations are used to find the zero temperature jamming threshold, ϕ_j , for soft, bidisperse disks in the presence of small fixed particles, or “pins”, arranged in a lattice. The presence of pins leads, as one expects, to a decrease in ϕ_j . Structural properties of the system near the jamming threshold are calculated as a function of the pin density. While the correlation length exponent remains $\nu = 1/2$ at low pin densities, the system is mechanically stable with more bonds, yet fewer contacts than the Maxwell criterion implies in the absence of pins. In addition, as pin density increases, novel bond orientational order and long-range spatial order appear, which are correlated with the square symmetry of the pin lattice.

1 Introduction

Over two decades ago, it was first proposed [1–3] that soft and granular materials can have a jammed, solid phase, which forms at sufficiently high packing fraction or pressure, and sufficiently low shear and temperature. Now, much is known about materials in the vicinity of the critical “Point J”; not only for simple models like soft or hard repulsive, frictionless spheres [4–7], but for particles which are non-spherical [8–12], have rough and/or frictional surfaces [13, 14], are confined within various wall geometries [15–17] and even active matter [18–20] (including work on active matter in the presence of fixed obstacles [21]). For frictionless soft spheres, a mixed first-second order phase transition, with upper critical dimension of $d = 2$ occurs [6, 22–24] at a maximally random close packing fraction (MRP). Near Point J, there are diverging length scales [25–29] and universal critical exponents for quantities like contact number, static and dynamical length scales, characteristic phonon frequency, and shear viscosity below the transition [6, 22, 30–33] - while exponents for elastic moduli depend on microscopic details like inter-particle potential [4, 22]. (A scaling relation for elastic energy has been shown to unify our understanding of the various critical exponents above the jamming transition [34].) At zero temperature and shear, the critical density ϕ_j represents a state of marginal stability, where according to Maxwell’s counting argument, the number of inter-particle contacts equals the number of unconstrained degrees of freedom. For $d = 2$, this situation of isostaticity, given translational invariance and a positive bulk modulus, implies [23]

that the typical number of contacts experienced by one of N particles is $z_c = 2d - 2/N$.

How then, will this maximally random, marginally stable structure be altered if particles are, in part, supported by elements internal to the system? For the case of quenched disorder via randomly-placed attractive sites, it was proposed [35] that disorder constitutes a fourth axis of the phase diagram ... altering the position of ϕ_j , as well as introducing a new critical threshold ϕ_p for the pinning of the flow of particles under an applied force. (Because flow has been shown to be impeded both by attractive [35] and repulsive obstacles [36, 37], there is some leeway as to whether one uses the term “pinned” or “clogged” to describe the state of arrested particle flow, with its distinctive heterogeneous geometry and time lag over which the flow comes to a halt. For both types of obstacle, the state of arrested flow becomes a true jammed state in the limit of large packing fractions [37].) Two different protocols for freezing particle positions as the jammed solid forms have been studied in Ref. [38]. One protocol produces over-coordinated systems, a consequence being qualitative changes in the characteristic frequency of soft modes, linked to the length scale above which a system is hyperstatic [25]. Applications to separation and sorting benefit from understanding flow in the presence of repulsive or attractive pinning sites [39]. Moreover, periodic arrangements of pins add an element of symmetry which can lead to predictable trends in kinematics studies, like the reduction of friction that accompanies kink propagation in driven colloidal solids [40] or directional locking in clogging simulations [36, 41]. Here, as in those references, we study periodically placed pins. Our pins are diminutive and softly repulsive, serving only to exclude volume. Our goal is to calculate the $T = 0$ jamming threshold as a function of pin density: equivalently, as a function of pin separation, the lattice constant, a . We also calculate structural quantities: contact number

^a Dept. of Physics and Astronomy, Swarthmore College, Swarthmore, PA 19081, USA. Fax: 01 610 328 7895; Tel: 01 610 328 8257; E-mail: abug1@swarthmore.edu

^b Dept. of Physics and Astronomy, University of Pennsylvania, Philadelphia, PA 19104, USA.

* Corresponding author

‡ Present address: Dept. of Mathematics, Cornell University, Ithaca, NY 14853, USA.

z , the distribution of bond angles, pair correlation function $g(r)$, fraction of unsupported particles (“rattlers”), the tendency of the bidisperse particles to size-segregate, and the scattering function $S(\vec{k})$ with \hat{k} referred to lattice symmetry axes. These permit us to see whether, as a function of a , the pins impose a modicum of order on what would otherwise be a highly isotropic, disordered solid.

2 Methods

M pins are placed on a square lattice in a 1×1 simulation cell with periodic boundary conditions. $N = N_l + N_s$ large and small particles are placed at random positions within the box, so that the packing fraction before equilibration is $\phi = N_s \pi r_s^2 + N_l \pi r_l^2$ with $N_s = N_l$ and $r_l/r_s = 1.4$, a ratio chosen to inhibit the tendency to form a hexagonal lattice[28] in $d = 2$. Pin radii r_{pin} are much smaller than those of particles; $r_{pin} = r_s/1000$, and variation around this value had a negligible effect on results. All particles in our system are soft disks, with a short range harmonic interaction potential given by

$$V = \begin{cases} 0 & r_{ij} > d_{ij} \\ \frac{1}{2} \varepsilon (1 - \frac{r_{ij}}{d_{ij}})^2 & \text{otherwise} \end{cases}, \quad (1)$$

where r_{ij} is the distance between the centers of particles i and j , d_{ij} is the sum of the radii of the two particles, and $\varepsilon \equiv 1$ for this zero-temperature study. It is known that the probability distribution of jamming thresholds is protocol-dependent [42, 43]. Structural and scaling properties may be noticeably different if the protocol yields a jammed configuration which is hyperstatic [44]; and even if isostatic, if the starting configuration is a hard-particle liquid exceeding a certain packing fraction[45]. We adopt a simple, athermal protocol which, in the absence of pins, is expected to yield a jamming transition at the lowest limit of any “line” of jamming thresholds[20], with the canonical structural and scaling properties described in O’Hern et al. [4]. The energy of a random configuration of soft discs is minimized via a conjugate gradient algorithm[46], after which configurations are tested for mechanical stability, and unsupported particles (“rattlers”) are removed. 1000 random seeds are used to generate initial particle configurations for each $[M, N]$ pair. Packing fractions ϕ are chosen to completely span the jamming transition for a given value of M .

The simulation halts when a chosen tolerance for changes in the gradient of the energy is reached. For the data discussed below, we not only assert that particles in a jammed solid are mechanically stable, but we ask that the system “percolates”, so that there is a connected path between box top and bottom sides, and between left and right sides. This criterion is not needed in the absence of pins, when mechanical stability occurs only if the system percolates. It is, however, a needed criterion in systems like that of Ref. [47], in which a short-ranged attraction between jammed particles permits the creation of non-spanning rigid clusters. Figures 1a, 1b illustrate two final configurations in a system with $M = 144$, hence $a = 0.0833$. This is sufficiently close to the particle size ($r_s = 0.0260382$) that, at jamming, equilibration may result in situations like Figure 1a, where no cluster of non-rattlers spans the system from left to right. At the highest pin density dis-

cussed below, approximately 1/4 of jammed configurations fail to percolate. Non-percolating equilibrated configurations like Figure 1a were excluded from further analysis.

In jamming protocols in which the transition is approached in a simulation cell of fixed size, finite-size effects are traditionally studied by adjusting particle radii in order to vary ϕ for a given value of N . However, the pin lattice introduces a new length scale, the pin separation $a = 1/\sqrt{M}$. To understand the effect of varying M , and hence the pin separation, without changing its relationship to the size of the particles, we employed a second protocol: fixing r_s and r_l for a set of M values, and instead, varying N in order to change ϕ . The range of N values did not need to be large (less than 10% for any value of M) in order to span the phase transition. With either protocol (rather than one where the system is relaxed from an initially overjammed configuration) sometimes the minimization procedure is not precise enough to identify a very slightly unstable configuration as such. Thus, we discard a very small fraction (less than 1%) of configurations with an insufficient number of bonds, N_{iso} , required to satisfy the number of degrees of freedom. These must necessarily have zero vibrational frequency modes, and be unstable. In packings without pins, we have checked that this criterion perfectly identifies a group of packings which also have unusually high energies and zero (or negative) bulk moduli.

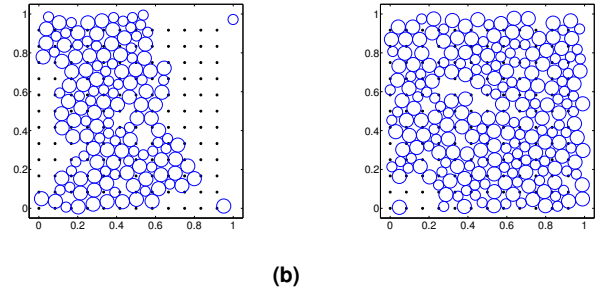


Fig. 1 Configuration of $N = 249$ particles and $M = 144$ pins that (a) jams, but does not percolate, and (b) jams and percolates. Pins are enlarged for visibility.

3 Results

3.1 Jamming probability

We examine the jamming transition by calculating $P_j(\phi)$, the probability of jamming as a function ϕ for different system sizes N , and different numbers of pins, M . A sigmoidal fitting form which estimates the center, ϕ_j , and width, w is:

$$P_j(\phi) = \frac{1}{(1 + b e^{(\phi_j - \phi)/w})^{1/b}}. \quad (2)$$

Eq. 2 is a Richards sigmoid which, for $b = 1$ is a simple, logistic sigmoid. This 2-parameter logistic sigmoid is used for $M = 0, 36, 81$ and 100 . For $M = 144, 169$, the deviation from $b = 1$ is significant in order to account for anisotropy about ϕ_j ; and thus the 3-parameter form of Eq. 2 is utilized.

Figure 2 and Table 1 illustrate that the two protocols yield consistent results for P_j in the limit of small M . However, there is a

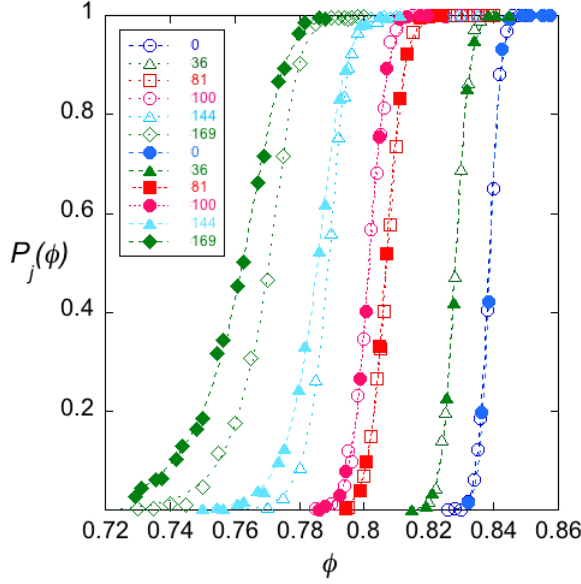


Fig. 2 $P_j(\phi)$ for systems with number of pins, M , given in legend and $N = 256$ particles (first protocol, open symbols) and $N \in [231, 261]$ particles (second protocol, closed symbols). Dashed lines indicate sigmoidal fits.

difference in the two protocols for the densest pin lattices. As M becomes comparable to N , the second protocol (which preserves the ratio of a to the particle size) yields a lower ϕ_j , and also yields a transition which becomes steadily wider as M increases. Unless otherwise noted, data discussed henceforth were calculated with the second protocol.

Number of pins	Second Protocol ϕ_j, w	First Protocol ϕ_j, w
$M = 0$	$0.838 \pm 1, 0.0018 \pm 2$	$0.838 \pm 1, 0.0020 \pm 2$
$M = 36$	$0.828 \pm 1, 0.0022 \pm 2$	$0.828 \pm 1, 0.0022 \pm 2$
$M = 64$	$0.820 \pm 1, 0.0022 \pm 2$	$0.8208 \pm 1, 0.0022 \pm 2$
$M = 81$	$0.807 \pm 1, 0.0027 \pm 2$	$0.8078 \pm 1, 0.0028 \pm 2$
$M = 100$	$0.802 \pm 1, 0.0028 \pm 2$	$0.802 \pm 1, 0.0028 \pm 2$
$M = 144$	$0.787 \pm 1, 0.0036 \pm 3$	$0.790 \pm 1, 0.0025 \pm 3$
$M = 169$	$0.766 \pm 2, 0.0046 \pm 4$	$0.773 \pm 2, 0.0033 \pm 3$

Table 1 Calculated critical point ϕ_j , and width w of transition, using sigmoidal fit to 1000 realizations per ϕ value. Systems contained M pins and $N \approx 256$ particles before equilibration.

As with other phase transitions, the jamming transition is only sharp in the thermodynamic limit, but finite-size scaling (FSS) allows one to approach this limit systematically to infer critical properties from simulations. As is true in the absence of pinned particles[23, 24, 48], results for finite- N can be collapsed onto one scaling curve. (A further scaling behavior with n_f has been proposed in the limit of extremely dilute, fixed particles[48].) Figure 3a shows $P_j(\phi)$ for four cases corresponding to different numbers of pins, but approximately the same pin density $n_f \equiv M/N$. In this case, $n_f \approx 0.14$. (Use of our second proto-

col requires us to utilize an N value which varies slightly, as will the density of pins n_f , with ϕ . However, n_f is constant to two significant figures for the data shown.) Values of N shown range from 64 to 1024. At $N = 64$ this rescaling fails, just as for small systems in previous studies [4]. Corrections to scaling would be necessary to collapse the data in $2d$ even without pins[49]. Fig. 3b shows that FSS can be a successful procedure to collapse data when, for sufficiently large systems and moderate pin densities, one plots P_j as a function of the rescaled distance to the critical point: $(\phi - \phi_j(N, n_f)) N^{1/2}$. The rescaling exponent $1/2$ is determined from the width at half maximum of the distribution of jamming thresholds [4].

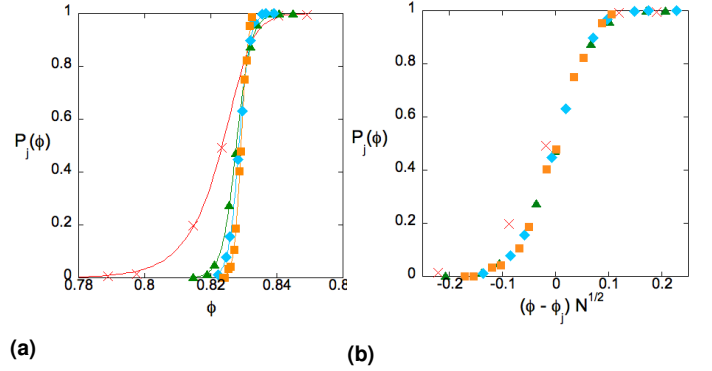


Fig. 3 Jamming at a pin density of $n_f = 0.14$ for four systems of different size regimes, with $N \approx 64$, $M = 9$ (red crosses), $N \approx 256$, $M = 36$ (green triangles), $N \approx 455$, $M = 64$ (aqua diamonds) and $N \approx 1024$, $M = 144$ (orange squares). (a) Probability of jamming as a function of packing fraction. Richard's sigmoid fit: $N \approx 64$, logistic sigmoid fit: $N \approx 256, 455, 1024$. (b) FSS version of (a), illustrating collapse of P_j data for three sufficiently large N values.

From the values of ϕ_j in Table 1, one might attempt to calculate a critical exponent for the correlation length $\xi \sim (\phi - \phi_j)^{-\nu}$; as it has been argued [35, 48] that jamming occurs when the inter-pin separation is equal to the correlation length. In d dimensions, pins will lower the jamming threshold by the amount:

$$\Delta\phi_j(n_f) \equiv \phi_j(n_f) - \phi_j(0) \propto n_f^{1/d\nu}, \quad (3)$$

Here $d = 2$, so a linear fit of $\Delta\phi_j(n_f)$ implies that $\nu = \frac{1}{2}$, consistent with previous findings[35, 37, 48]. Figure 4 suggests that for $n_f \leq 0.25$, the data is approximately linear; a power law fit yields $|\Delta\phi_j(n_f)| \propto n_f^\alpha$ with $\alpha = 0.91$ and $\alpha = 0.95 \pm 0.10$ for $N = 256, 1024$ respectively. If we assume that $\alpha = 1$ (linear fit) the slope is $\frac{\partial\phi_j}{\partial n_f} = -0.071, -0.072 \pm 0.002$ for $N = 256, 1024$ respectively. (This slope seems to depend on the form of the interaction between particles and pinned obstacles[35, 37, 48].) The deviation of the data in Fig. 4 from linearity at higher n_f suggest that sufficiently dense, ordered pins do more than single out the correlation length of a highly random packing*. Below, we show that there is an onset of both local (bond) and global (positional) ordering as the pin

* Preliminary data indicate that, further, the rule of monotonic decrease seen in Fig. 4 can be violated. These will appear in a forthcoming publication.

lattice density increases.

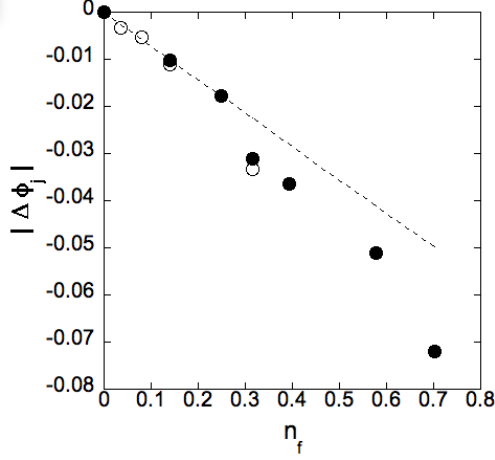


Fig. 4 Deviation of jamming threshold from the zero-pin value, as a function of pin density n_f . Filled circles: $N \approx 256$, open circles: $N = 1024$ which are taken with the first protocol, but at sufficiently small n_f where (Table 1) the two methods are not demonstrably different. Error bars are smaller than data points. Linear fit with slope -0.071 is shown, as is consistent with data for $n_f \leq 0.25$.

3.2 Angular and spatial ordering

Two particles whose radii overlap can be thought of as sharing a “bond”, oriented in the direction between the particle centers. The geometry of the bond network is central to the theory of jamming; controlling the fragility of the jammed state, elastic properties, the phonon spectrum, scaling exponents, and evolving in response to compression and shear[2, 50, 51]. The angle formed by a pair of bonds which carry the largest forces reveals a distribution which supports the picture of “force chains” [52, 53]. In the presence of pins, we must first ask a more basic question about individual bonds: Are these isotropically distributed in angle space? Rather than answering in terms of the pin-to-particle ratio n_f , it is more revealing to use the dimensionless ratio of particle-to-pin sizes: $\lambda = r_s/a$. By the definition of the box volume per pin, λ is related to ϕ and n_f via:

$$\lambda^2 = \pi \frac{1 + 1.4^2}{2} \phi n_f. \quad (4)$$

While Eq. 4 is always true, it is relevant to tabulate $\lambda \equiv \lambda_j$ at the jamming threshold for a particular value of n_f . Table 2 holds values found in the current work. In this way, one can relate the horizontal axes of Fig. 4 and Fig. 6.

Figure 5 compares the distribution of bond angles with $N \approx 256$ systems for various pin densities. One sees the distribution become progressively more anisotropic as M increases. The distribution of bonds $P(\theta)$ has fourfold symmetry as one expects given a square pin lattice. (Figure 5 only shows angles in the range $\theta \in [0, \pi/2]$; bonds with $\theta \in [\pi/2, \pi]$ are averaged with the data shown.) The reflection symmetry about $\theta = \pi/4$ is clear.

Figure 6 shows the order parameter $\langle m \rangle \equiv \langle e^{i4\theta} \rangle$ as a func-

M	n_f	λ_j
0	0.000	—
36	0.141	0.158
64	0.250	0.208
81	0.316	0.234
100	0.394	0.260
144	0.578	0.312
169	0.701	0.338

Table 2 The number of pins, M , and $r_s/a \equiv \lambda_j$ corresponding to $n_f = M/N$ evaluated at ϕ_j .

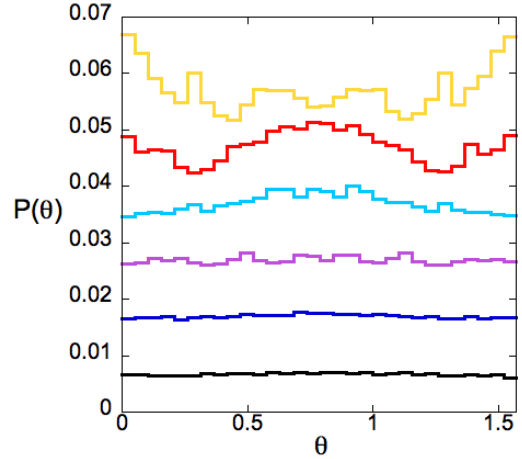


Fig. 5 Histograms proportional to the probability $P(\theta)$, that a bond makes angle θ with the x-axis. Each data set corresponds to the system parameters closest to the fraction at jamming ϕ_j from sigmoidal fits, and given Table 1). Different numbers of pins M corresponding to different size ratios at jamming λ_j are shown in black: $M = 0$, $\lambda_j = 0$; dark blue: $M = 36$, $\lambda_j = 0.158$; purple: $M = 81$, $\lambda_j = 0.234$; light blue: $M = 100$, $\lambda_j = 0.260$; red: $M = 144$, $\lambda_j = 0.312$; and yellow: $M = 169$, $\lambda_j = 0.338$. Histograms for successive parameter values are displaced from each other vertically by 0.01 for ease of viewing.

tion of $\lambda = r_s/a$ for $N \approx 256$ systems. The magnitude of the real part of this order parameter, given the choice of axes, is approximately equal to $|\langle m \rangle|$. Apparently, an angular ordering transition occurs somewhere between $\lambda = 0.234$ and 0.260 . While $|\langle m \rangle|$ continues to increase above the transition, note the change in sign of $\text{Re} \langle m \rangle$ at the densest lattice studied (yellow curve in Figure 5) which correlates with the change in the most-probable bond angle from $\theta = \pi/4$ for less dense lattices, to $\theta = 0, \pi$. While it appears that $\langle m \rangle$ is nonzero for all values of $a > 0$ studied, this may be a finite-size effect having to do with the square simulation cell with periodic boundary conditions, which creates a slight amount of ordering even for $a = 0$. As a check on this, the inset of the figure shows both $N = 256$ and 1024 data for $a = 0, 0.167$. In the latter case (open symbols) the order parameter is significantly closer to zero. The $T=0$ jamming transition constitutes an out-of-equilibrium, phase transition. Nevertheless, the abrupt increase in $|\langle m \rangle|$ with cubic ordering from pins is reminiscent of a phase transition, such as the isotropic to nematic transition in uniaxial liquid crystals in the presence of an

orienting field [?]. Statistical ensemble ideas have successfully described jamming [54] and perhaps will allow one to map out a bond ordering transition using pin density as a control parameter.

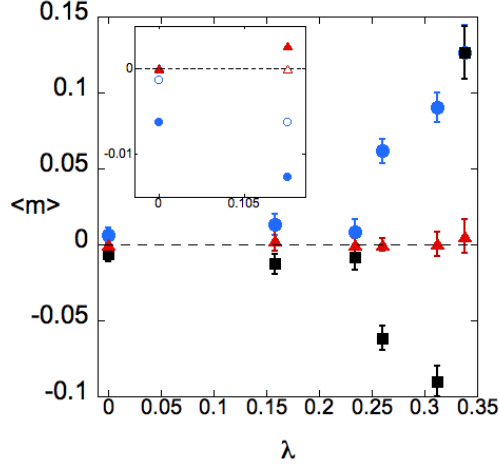


Fig. 6 Order parameter, $\langle m \rangle$, as a function of particle-lattice size ratio, λ . Black squares: $Re \langle m \rangle$, red triangles: $Im \langle m \rangle$, and blue circles: $|\langle m \rangle|$. Inset: Real and imaginary parts of $\langle m \rangle$ showing both $N = 256$ (solid symbols) and $N = 1024$ (open symbols) data.

A bidisperse distribution results in particle-size-dependent preferences for certain bond angles. Thus, detailed features of $P(\theta)$ in Figure 5 can be traced to bonds between particles of specific sizes, as exemplified in Fig. 7. The large-large bonds tend to be oriented

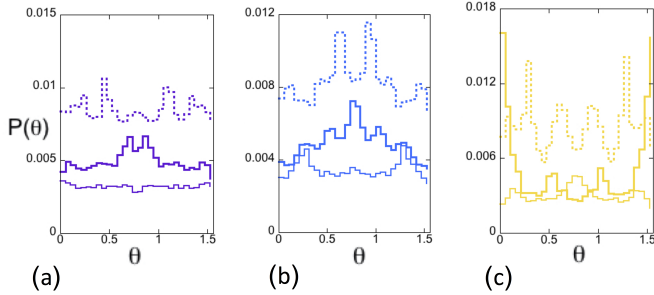


Fig. 7 $P(\theta)$ for different types of bond. Thick lines: large-large, thin: small-small, dotted: large-small. Colors indicating M value are as in previous figures. a) purple: 81; b) light blue: 100; c) yellow: 169.

near $\theta = \pi/4$ for $M = 81, 100$; however a couple of other favorable orientations appear as side peaks in Figs. 7a,b. At the highest pin density studied, $M = 169$ in Fig. 7c, large-large bond probabilities have a peak at approximately $\theta = \pi/6, 2\pi/3$, which is also true for $M = 100$. But for $M = 169$, the most probable large-large bond orientation is horizontal or vertical. In contrast, for $M = 169$ the small-small bond angles have a preferred orientation of $\theta = \pi/4$. Small-small bonds show little orientational structure at $M = 81$, and at $M = 100$ are most likely to be oriented at $\theta = \pi/12, 5\pi/12$; coinciding with one set of large-large bond peaks. Large-small bond probabilities have a small local maximum at $\theta = \pi/4$ for

$M = 81$. But their orientations are most likely to fall at other angles for all M values shown in Fig. 7. The take home message is that the details of the bond angle distribution depend in an intricate way on particle sizes r_s, r_l and pin separation, a . It is worth noting that there is only a slight degree of particle size segregation; whether same-sized or differently-sized particles are more likely to share a contact varies only slightly with M . Segregation is largest at $M = 169$, where differently-sized particle contacts exceed same-sized ones by 4%.

The pair correlation function between particle centers, $g(r)$ with $r_s = 0.0133$, and $r_l = 0.0186$ is shown in Fig. 8 for $N = 1024$ particles - with zero pins (blue) and $M = 144$ pins (red), so that $a = 0.0833$. At the modest pin density $n_f = 0.141$ (the fourth open data point in Fig. 4 and second data point in Fig. 6) Fig. 8a indicates that pins do not change $g(r)$ at distances r which are within the first few “solvation shells” of a reference particle. Structure related to the bidisperse system is visible; for example, the first three peaks correspond to $r \approx 2r_s, r_s + r_l$, and $2r_l$. However, as seen in Fig. 8b, pins are responsible for the persistence of this order across the simulation cell. These regular oscillations in $g(r)$ have a spatial period of 0.030 ± 0.005 , the typical separation between neighboring particles. These oscillations feature an amplitude modulation, which can be explained by the superposition of contacts at large-large, large-small, and small-small contact distances: 0.037, 0.032, 0.027. The width of the “beat pattern” of three such superposed sinusoids is quite comparable to the value of 0.20, seen in Fig. 8b. Fig. 9 data have $N \approx 256$,

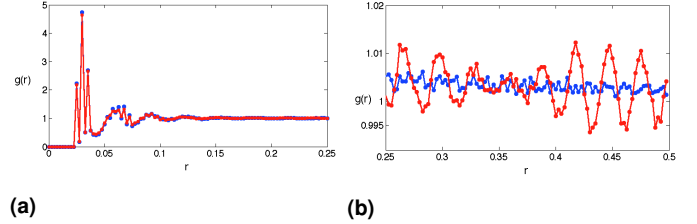


Fig. 8 Pair correlation function, $g(r)$ for $N = 1024$ particles at the jamming threshold. Blue symbols: $M = 0$. Red symbols: $M = 144$.

$r_s = 0.0260$, $r_l = 0.0364$, with no pins for the blue curve, while for the yellow curve $a = 0.0769$. At this large pin density $n_f = 0.698$ (corresponding to the the final data points in Figs. 4 and Fig. 6) the pins slightly reduce the spatial period, and pin-induced oscillations in particle density are perceptible throughout the entire range of r values.

Structure seen in $g(r)$ readily translates to its Fourier transform, $S(\vec{k})$. In the presence of a pin lattice, $S(\vec{k})$ for vector \vec{k} will reveal the long range order in structurally-relevant directions. For a perfect square lattice, these directions would simply be all integers $[h \ l]$. We would expect some evidence of these directions to be present in $S(\vec{k})$ in systems where pins produce order. We define a normalized scattering intensity as this structure factor:

$$S(\vec{k}) = \frac{1}{N} \sum_{j=1}^N \sum_{k=1}^N e^{-i\vec{k}(\vec{R}_j - \vec{R}_k)} \quad (5)$$

where the sums in Eq. 5 extend over pairs of particles.

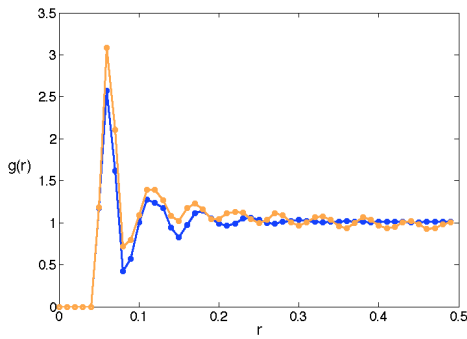


Fig. 9 Pair correlation function, $g(r)$ for particles at their jamming threshold. Blue symbols: $N = 266$, $M = 0$, yellow symbols: $N = 241$, $M = 169$.

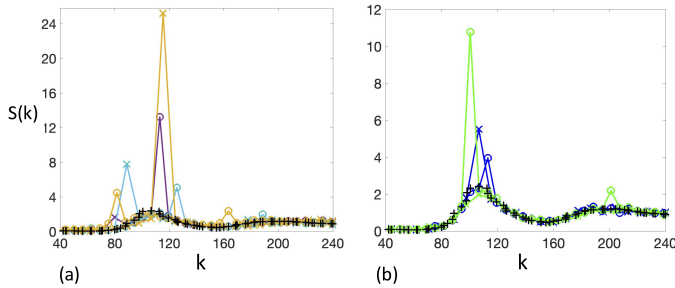


Fig. 10 Particle scattering function $S(\vec{k})$ vs. wave number k , in units where the box is of linear size 1. Colors indicating M value are: Black: 0, dark blue: 36, green: 64, purple: 81, light blue: 100, yellow: 169. The + symbols signify $M = 0$ data. For other M values, crosses signify \vec{k} oriented at 45° with respect to the row direction of the pin lattice; circles signify \vec{k} oriented at 0° .

The structure factor $S(\vec{k}) \equiv S(k)$ for zero pins is shown with + symbols in Fig. 10, while circles in Figs. 10a, b depict $S(k_{10})$ where $k_x = k$, $k_y = 0$ and crosses depict $S(k_{11})$, where $k_y = k_x = \sqrt{2}k$. Colors indicate M values. Discretization due to the periodic boundaries of the 1×1 simulation cell restricts the resolution in k space to $\Delta k = 2\pi$. The horizontal scale is chosen to focus on the region relevant to the first peak of $g(r)$ as seen in Fig. 9. A peak from particles separated by precisely $2r_s$, $r_s + r_l$ or $2r_l$ along each lattice direction would fall roughly at $k = 121$, 101 or 86. The main message of Fig. 10 is the existence of lattice-induced peaks which are correlated with the positions of pins. Were it simply the case that particles took on the crystalline symmetry of a perfect square, peaks would fall at the reciprocal lattice vectors $k_x = n\Delta k$, $k_y = m\Delta k$ with n, m integers. Small amounts of positional disorder and finite size effects from simulation would result in recognizable modulation of peak heights and widths [55]. For our finite system the peaks for $n = m = 1$ and $n = 1$, $m = 0$ would be equal in height. However, Fig. 10 shows that the structure induced by pins is quite different.

The locations of peaks in Fig. 10a, signify particles whose separation, projected onto the direction of \vec{k} , is half of the inter-pin spacing. For $M = 81$, $a = 0.111$: The large peak (circle) at $k = 113$, implies $2\pi/k = a/2$. The much smaller peak (cross) at $k = 80$ implies $2\pi/k = \sqrt{2}a/2$. For $M = 100$, $a = 0.1$: Peaks (circles) fall at $2\pi/k = a$, $a/2$ and $a/3$, with the largest peak indicating two particles per lattice unit cell; similarly for the large peak (cross) at

$k = 89 = \sqrt{2}a/2$. For $M = 169$, $a = 0.0769$: Once again, a dominant peak (cross) at $k = 115.5$ indicates two particles per lattice unit cell projected along a 45° angle.

At the pin densities shown in Fig. 10a, a pair of bidisperse particles, in contact but non-overlapping, do not in general “fit” within an $a \times a$ square region with pins at its four vertices. For example, for $M = 81$, large-small and large-large pairs fit with their bond oriented at 45° but not horizontally. Analyzing these data presents an enormously complicated packing problem, even if only particle pairs are considered. Without solving further, one can only speculate that such packing constraints drive the qualitative shift from ordering in the horizontal or vertical directions, to ordering along a diagonal in the lattice. On the other hand, the trend shown in Fig. 7 for bond angles is *opposite*, with a bond probability density maximum at $\theta = 45^\circ$ at lower pin densities, which has shifted to $\theta = 0$ at higher densities. Local bond and long-range positional order are, broadly speaking, two distinct results of the pin lattice.

Supporting this notion is the fact that the more dilute pin lattices are also able to promote long-range positional order. This is seen in Fig. 10b, which depicts the two lowest pin-densities studied. These have no significant bond order according to Fig. 6. For $M = 36$, $a = 0.167$: The peak (circles) at $k = 113.09$ give $2\pi/k = 0.0556 = a/3$. The naïve picture is one of three particles spanning a lattice unit cell horizontally (or vertically). The peak (crosses) at $k = 106.6292$ implies $2\pi/k = 0.0589 = a\sqrt{2}/4$, leading to a naïve picture of four particles spanning the diagonal of the lattice unit cell. For $M = 64$, $a = 0.125$: There is no evidence of lattice-induced structure (crosses) in the 45° direction. However, a large peak (circle) at $k = 100.5$ implies structure in the horizontal (or vertical) direction with period $2\pi/k = 0.0625 = a/2$.

The take-away is that the order produced by the pins is mired in the details of the packing of bidisperse particles. It is difficult to find a case where local bond order and global spatial order transparently reinforce each other. For example, a bond angle $\theta = \pi/4$ is favored for $M = 100$ via a broad peak and directly via large-large bonds in Fig. 7. However, no type of $M = 81$ bond pair shows a preference for $\theta = 0$, while Fig. 10a shows its most dramatic peak in that lattice direction. There is every reason to suppose that $S(\vec{k})$ in lattice directions other than 0° or 45° will yield additional structural features, due to the detailed way these particles pack among the pins.

3.3 Contact statistics

How do pins affect a particle’s average contact number, $z = z_{pp} + z_{pf}$? Here, the subscript “pp” denotes a contact between particles and “pf” denotes contact between a particle and a fixed pin. z_{pp} for a fixed value of ϕ is reduced by pins, in part because a particle which touches only two other particles may contribute to the jammed solid, if stabilized by a pin. Fig. 11 is typical of the probability distributions $P(z)$ and $P(z_{pp})$. Figs. 11a and 11b show that increasing the number of pins from $M = 81$ to 144 at a fixed value of ϕ changes the distribution only slightly, increasing the average contact number from $z = 3.90$ to 4.01, and from $z_{pp} = 3.59$ to 3.61. In Figs. 11c and 11d, a more dramatic change

in contact statistics is seen, when a comparison is made between systems at their respective values of ϕ_j . The average contact number now *decreases* as pin density increases, from $z = 3.90$ to 3.73 , and from $z_{pp} = 3.59$ to 3.29 .

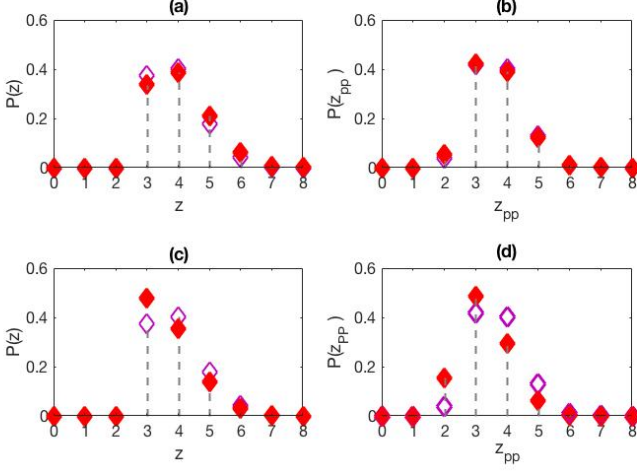


Fig. 11 Probability that particle has z contacts. Open diamonds: $M = 81$. Filled diamonds: $M = 141$. (Colors correspond to M as in earlier figures.) a) and b) depict $\phi = 0.807$; c) and d) depict $\phi = \phi_j(M)$. (See Table 1.) a) and c) include all contacts; b) and d) only particle-particle contacts.

The traditional Maxwell counting argument [23] asserts that frictionless, spherical particles require a minimum of $N_{B\text{ iso}} = dN - qd + 1$ bonds. The second term in this definition arises from d zero modes associated with global translations, while the third term ensures a positive bulk modulus. Here, $q = 1$ without pins, but $q = 0$ if even one pin is present, as our equilibration protocol breaks translational symmetry [48]. Say that the total number of bonds is $N_B = N_{pp} + N_{pf}$. The number of excess bonds between particles is found via a generalized isostaticity criterion [38]:

$$N_{B\text{ excess}} \equiv N_B - N_{B\text{ iso}} = N_{pp} + N_{pf} - dN + qd - 1. \quad (6)$$

Without pins, $z_{\text{iso}} = 2d - (2/N) = 2N_{B\text{ iso}}$. In the presence of pins it is no longer true that one can write $z_{\text{iso}} \propto N_{B\text{ iso}}$, as N_{pp} bonds stabilize two particles, and N_{pf} bonds stabilize only one.

Hyperstaticity, by which one means $N_B > N_{\text{iso}}$, is expected in certain cases, such as frictional particles [13], or those with attractive interactions [47]. We see increasing hyperstaticity with n_f , reminiscent of previous work with frozen particles [38] as well as in bidisperse mixtures in which the ratio of small to large radii is varied [56]. However, even at $n_f = 0$, there is a slight excess of contacts/bonds - a result of a protocol which fixes λ for a set of initial conditions, thus creating realizations at various distances from their individual jamming points. (As one might expect, this fraction of excess bonds is independent of the system size, N .) Thus, Fig. 12 shows $N'_{B\text{ excess}} \equiv N_{B\text{ excess}} - N_{B\text{ excess}, n_f=0}$. Though $N'_{B\text{ excess}}$ rises as pin number rises, the number of excess bonds per pin is found to decrease. That is, $N'_{B\text{ excess}} \propto n_f^\beta$, with $\beta = 0.61 \pm 0.07$. That the number of excess bonds scales approximately as the square root of the number of pins is reminiscent

of a surface term. Since both z and z_{pp} decrease with increasing pin density, it is the number of bonds between particles and pins, N_{pf} , which increases in the vicinity of ϕ_j . The number of excess bonds reflect the interplay between the contact statistics (rising numbers of contacts between particles and pins) and the falling number of non-rattler particles near ϕ_j (as seen in Fig. 13).

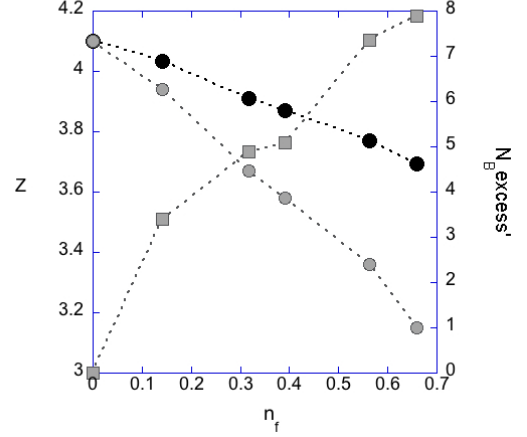


Fig. 12 Typical number of contacts per particle. Black circles: All types of contacts, z , grey circles: Particle-particle contacts, z_{pp} , grey squares: $N'_{B\text{ excess}} - N_{B\text{ excess}, n_f=0}$.

Figs. 4 and 12 indicate that pins provide a parsimonious route to jamming, in that ϕ_j is lower and fewer contacts are needed for stability as the density of pins increases. Since ϕ_j is traditionally pitched as a critical initial packing fraction, one should also ask about the final packing fraction, after removal of particles which do not alter the mechanical stability (or percolation) of the system. In Fig. 13, one sees the fraction of such rattlers for various initial packing fractions, ϕ . As one expects, small particles are more likely to be rattlers, than are large particles[56]. At the

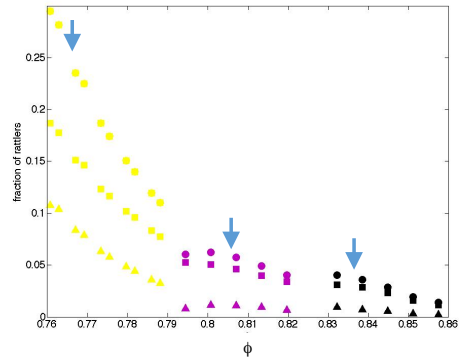


Fig. 13 Fraction of rattlers as a function of initial packing fraction. Colors as in Fig. 5 are black: $M = 0$, purple: $M = 81$ and yellow: $M = 169$. Fraction of rattlers by size are shown as circles: all rattlers, squares: small particles, and triangles: large particles. Blue arrows indicate the location of $\phi_j(M)$.

same initial packing fraction ϕ , there will be fewer rattlers for

higher densities of pins; since additional pins provide support for additional particles. If we compare systems at their respective ϕ_j , then for moderate pin densities, e.g. $M = 81$ in Fig. 13, there is no dramatic change in the fraction of rattlers at this threshold. However, as the density of pins approaches the highest values studied (pin separation almost comparable to particle size), the fraction of rattlers rises dramatically, as seen for $M = 169$ in Fig. 13. In this case, the reduction of ϕ_j is compounded by a reduction in non-rattlers: a jammed system with a final packing fraction of $\phi \approx 60\%$ for $M = 169$, as compared with $\phi \approx 80\%$ in the absence of pins.

4 Conclusions

Introducing a square lattice of pin-like obstacles to systems of bidisperse particles will lower the jamming threshold, ϕ_j . The threshold decreases linearly at low pin densities, and more steeply at higher densities. The pin lattice stabilizes configurations with not only lower initial packing fraction ϕ , but also lower contact number z and an increasing proportion of rattlers. There are additional, detailed changes in the structure of the jammed system as pin density increases. The distribution of bond angles becomes increasingly anisotropic and we see a transition in a cubatic order parameter when the ratio of particle diameter to pin spacing on the order of $1/2$. The bond angle distribution exhibits four-fold symmetry, consistent with the presence of pins in a square lattice, but with details that depend sensitively on the packing of bidisperse particles among pins of a given density. The presence of oscillations in the pair correlation function suggests long-range spatial ordering in the system. Peaks in the structure factor arise, locked to the spatial frequency of the pin lattice. In general, the axes along which there is long-range spatial order need not correspond to directions of preferred bond angles. This supports the notion that long-range, spatial ordering can be considered separately from local, bond ordering. Both are consequential when the pin separation is on the order of the particle size.

Conflicts of interest

There are no conflicts to declare.

Acknowledgements

We thank Tristan Cates, Carl Goodrich, and M. Lisa Manning for invaluable technical contributions. We thank Cacey Bester, Peter Collings, Randall Kamien, Andrea Liu, Cynthia Reichhardt-Olsen, Daniel Sussman, Brian Utter, and Katharina Vollmayr-Lee for their comments and insights. Acknowledgement is made to the donors of the American Chemical Society Petroleum Research Fund for partial support of this research and to the National Science Foundation: NSF Grant DMR-1905474. We are grateful to Swarthmore College's Provost, Division of Natural Sciences, and Individual Donors. A. L. Graves is grateful for a Michener Sabbatical Fellowship. S. Ridout has been supported by PGS-D fellowship from NSERC and the Simons Foundation Cracking the Glass Problem Collaboration award No. 45494 to Andrea J. Liu.

Notes and references

- 1 D. Durian, *Phys. Rev. Lett.*, 1995, **75**, 4780.

- 2 M. E. Cates, J. P. Wittmer, J. P. Bouchaud and P. J. Claudin, *Phys. Rev. Lett.*, 1998, **81**, 1841.
- 3 A. J. Liu and S. R. Nagel, *Nature*, 1998, **396**, 21.
- 4 C. S. O'Hern, L. E. Silbert, A. J. Liu and S. R. Nagel, *Phys. Rev. E*, 2003, **68**, 011306.
- 5 P. Olssen and S. Teitel, *Phys. Rev. Lett.*, 2007, **99**, 178001.
- 6 A. J. Liu and S. R. Nagel, *Annu. Rev. Condens. Matter Phys.*, 2010, **1**, 347.
- 7 A. O. N. Siemens and M. van Hecke, *Physica A*, 2010, **389**, 4255.
- 8 A. Donev, R. Connelly, F. H. Stillinger and S. Torquato, *Phys. Rev. E*, 2007, **75**, 051304.
- 9 M. Mailman, C. F. Schreck, C. S. O'Hern and B. Chakraborty, *Phys. Rev. Lett.*, 2009, **102**, 255501.
- 10 K. VanderWerf, W. Jun, M. D. Shattuck and C. S. O'Hern, *Phys. Rev. E*, 2018, **97**, 012909.
- 11 C. Brito, H. Ikeda, P. Urbani, M. Wyart and F. Zamponi, *PNAS*, 2018, **115**, 11736.
- 12 Y. Zhao, J. Barés, H. Zheng, C. S. Bester, Y. Xu, J. E. S. Socolar and R. P. Behringer, *arXiv:1902.08024v1*, 2019.
- 13 L. E. Silbert, *Soft Matter*, 2010, **16**, 2918.
- 14 R. P. Behringer, *Granular Materials*, 2015, **16**, 10.
- 15 K. W. Desmond and E. R. Weeks, *Phys. Rev. E*, 2009, **80**, 051305.
- 16 S. S. Ashwin and R. K. Bowles, *Phys. Rev. Lett.*, 2009, **102**, 235701.
- 17 S. Torquato and F. H. Stillinger, *Rev. Mod. Phys.*, 2010, **82**, 2633.
- 18 S. Henkes, Y. Fily and M. C. Marchetti, *Phys. Rev. E*, 2011, **84**, 040301.
- 19 D. Bi, J. Lopez, J. Schwarz and M. L. Manning, *Nature Phys.*, 2015, **10**, 1074.
- 20 N. Xu and Q. Liao, *Soft Matter*, 2018, **14**, 853.
- 21 C. Reichhardt and C. J. Olsen Reichhardt, *Phys. Rev. E*, 2014, **90**, 012701.
- 22 M. van Hecke, *J. Phys.: Condens. Matter*, 2009, **22**, 033101.
- 23 C. P. Goodrich, A. J. Liu and S. R. Nagel, *Phys. Rev. Lett.*, 2012, **109**, 095704.
- 24 C. P. Goodrich, S. Dagois-Bohy, B. P. Tighe, M. van Hecke, A. J. Liu and S. R. Nagel, *Phys. Rev. E*, 2014, **90**, 022138.
- 25 M. Wyart, S. Nagel and T. Witten, *Europhys. Lett.*, 2005, **72**, 486.
- 26 C. P. Goodrich, W. G. Ellenbroek and A. J. Liu, *Soft Matter*, 2013, **9**, 109933.
- 27 S. Shoenholz, C. P. Goodrich, O. Kogan, A. J. Liu and S. R. Nagel, *Soft Matter*, 2013, **9**, 11000.
- 28 C. Reichhardt and C. J. Olsen Reichhardt, *Soft Matter*, 2014, **17**, 2932.
- 29 D. Hexner, A. J. Liu and S. R. Nagel, *Phys. Rev. Lett.*, 2018, **121**, 115501.
- 30 L. Silbert, A. J. Liu and S. R. Nagel, *Phys. Rev. Lett.*, 2005, **95**, 098301.

- 31 M. Wyart, S. L. E., S. R. Nagel and T. A. Witten, *Phys. Rev. E*, 2005, **72**, 051306.
- 32 A. S. Keys, A. R. Abate, S. C. Glotzer and D. J. Durian, *Nature Physics*, 2007, **3**, 260.
- 33 P. Olssen and S. Teitel, *Phys. Rev. E*, 2011, **83**, 030302(R).
- 34 C. P. Goodrich, A. J. Liu and J. P. Sethna, *PNAS*, 2016, **35**, 9745.
- 35 C. J. Olson Reichhardt, E. Groopman, Z. Nussinov and C. Reichhardt, *Phys. Rev. E*, 2012, **86**, 061301.
- 36 H. T. Nguyen, C. Reichhardt and C. J. Olson Reichhardt, *Phys. Rev. E*, 2017, **95**, 030902(R).
- 37 H. Péter, A. Libál, C. Reichhardt and C. J. Olson Reichhardt, *Scientific Reports*, 2018, **8**, 10252.
- 38 C. Brito, G. Parisi and F. Zamponi, *Soft Matter*, 2013, **9**, 8540–8546.
- 39 C. Reichhardt and C. J. Olsen, *Phys. Rev. Lett.*, 2002, **89**, 078301.
- 40 T. Bohlein, J. Mikhael and C. Bechinger, *Nature Mater.*, 2012, **11**, 126.
- 41 C. Reichhardt and C. J. Olsen Reichhardt, *J. Phys.: Condens. Matter*, 2012, **24**, 225702.
- 42 P. Chaudhuri, L. Berthier and S. Sastry, *Phys. Rev. Lett.*, 2010, **104**, 165701.
- 43 T. Bertrand, R. Behringer, B. Chakraborty, C. S. O'Hern and M. D. Shattuck, *Phys. Rev. E*, 2016, **93**, 012901.
- 44 C. F. Schreck, C. S. O'Hern and L. E. Silbert, *Phys. Rev. E*, 2011, **84**, 011305.
- 45 M. Ozawa, T. Kuroiwa, A. Ikeda and K. Miyazaki, *Phys. Rev. Lett.*, 2011, **109**, 205701.
- 46 J. Schewchuk, *An Introduction to the Conjugate Gradient Technique Without the the Agonizing Pain*, Carnegie Mellon University technical report, 1994.
- 47 D. Koeze, L. Hong, A. Kumar and B. Tighe, *Elasticity of Jammed Packings of Sticky Disks*, 2020.
- 48 A. L. Graves, S. Nashed, C. P. Goodrich, A. J. Liu and J. P. Sethna, *Phys. Rev. Lett.*, 2016, **116**, 235501.
- 49 D. Vagberg, D. Valdez-Balderas, M. Moore, P. Olsoon and S. Teitel, *Phys. Rev. E*, 2011, **83**, 030303(R).
- 50 T. Majumdar and R. Behringer, *Nature*, 2005, **435**, 1079.
- 51 J. Zhang, T. Majumdar, M. Sperl and R. Behringer, *Soft Matter*, 2010, **6**, 1982.
- 52 J. Zhou and A. Dinsmore, *J. Stat. Mech.*, 2009, L05001.
- 53 K. Desmond, P. Young, D. Chen and E. Weeks, *Soft Matter*, 2013, **9**, 3424.
- 54 D. Bi, S. Henkes, K. F. Daniels and B. Chakraborty, *Annu. Rev. Condens. Matter Phys.*, 2015, **6**, 63.
- 55 A. Guinier, *X-ray Diffraction. In Crystals, Imperfect Crystals, and Amorphous Bodies*, W.H. Freeman and Co., London, UK, 1st edn., 1963, p. XXX.
- 56 D. Koeze, D. Vagberg, B. Tjoa and B. Tighe, *Europhys. Lett.*, 2016, **113**, 54001.